Design of K-Band CMOS Variable Gain Amplifier Using Amplification Stage and Variable Attenuation Stage

Junhyuk Yang[1], Seongjin Jang[1], and Changkun Park[1,2,a]
[1]Department of Electric Engineering, Soongsil University
[2]Department of Intelligent Semiconductors, Soongsil University
E-mail : huldo0702@soongsil.ac.kr, jsj0613@soongsil.ac.kr, pck77@ssu.ac.kr

***Abstract* - In this study, we design a K-band CMOS variable gain amplifier (VGA) for beamforming system applications. The designed VGA consists of amplification and attenuation stages. The amplification stage consists of two common-source gain stages and has a power gain of approximately 18 dB in the simulation. In the case of the attenuation stage, it has a total of 5-bit attenuation steps, and the attenuation range in the simulation is 31 dB. To suppress insertion loss, attenuation bits for low attenuation levels were designed in a distributed structure. On the other hand, attenuation bits for high attenuation levels are designed in a π-structure to secure high attenuation levels. In addition, to suppress the phase error, tail capacitors are added to transistors used in the attenuation stage. The designed K-band VGA was manufactured using a 65-nm RFCMOS process. The chip size of the designed VGA was 0.65 × 0.50 mm^2. At operating frequencies 22.0 GHz to 23.6 GHz, the measured variable gain range was between 26.5 dB and 28.2 dB. In this case, the measured RFM phase and attenuation errors were less than 6.40° and 1.24 dB, respectively.**

***Keywords*—Attenuator, beamforming, CMOS, variable gain amplifier**

I. INTRODUCTION

With the development of 5G mobile communication technology, beamforming systems are in the spotlight as one of the main transceiver structures of wireless communication systems [1–4]. Such a beamforming system is expected to be adopted not only in 5G but also in 6G mobile communication, and attempts are being made to apply it to various applications [5–7].

With the introduction of beamforming systems, interest in functional circuits that can adjust the beam patterns of antennas, such as phase shifters, variable gain amplifiers (VGAs), and attenuators, is also increasing. In particular, VGAs and attenuators played a major role in typical transceiver systems for mobile communication, and their importance has increased further in beamforming systems [8–11]. For such VGAs, the variable gain range and RMS phase and gain errors are the main performance indicators. Similarly, for attenuators, variable attenuation ranges and RMS phase and attenuation errors are the main performance indicators.

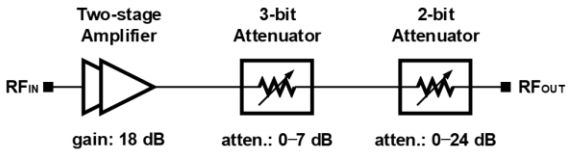

Fig. 1. Block-diagram of the designed VGS.

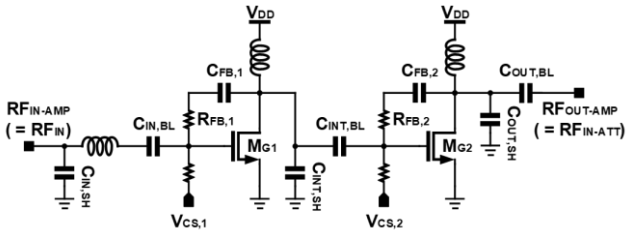

Fig. 2. Schematic of the amplification stage.

In this study, for the beamforming system in the flexible access common spectrum (FACS) applications [5–7], we designed a K-band CMOS VGA. In particular, we combined a gain amplifier and a digital step attenuator to simultaneously secure variable gain and variable attenuation function with a single integrated circuit (IC). In order to secure a sufficient gain, the gain amplifier was composed of two-stages. Here, in order to suppress the phase error due to the variation of the gain, a variable function was implemented only at the attenuation stage of the designed VGA. In addition, a digitally controllable attenuator was combined with a total of 5-bits to secure a sufficient variable gain range. To further suppress the phase error, tail capacitors were added to transistors used in the attenuation stage.

II. DESIGN OF THE K-BAND CMOS VGA

In this study, in order to secure both variable attenuation and gain functions at the same time, the VAG consisted of two stages and a 5-bit attenuator, as shown in Fig. 1. Here, the operating frequency was set from 22.0 GHz to 23.6 GHz. As follows, the gain amplification stages were first

a. Corresponding author; pck77@ssu.ac.kr

Manuscript Received Sep. 23, 2023, Revised Dec. 4, 2023, Accepted Dec. 5, 2023

This is an Open Access article distributed under the terms of the Creative Commons Attribution Non-Commercial License (http://creativecommons.org/licenses/by-nc/4.0) which permits unrestricted non-commercial use, distribution, and reproduction in any medium, provided the original work is properly cited.

TABLE I. Specific Values of the Devices Used in the Amplification Stage.

Device	Value	Device	Value
M_{G1}, M_{G2} (μm)	40[1)]	$C_{INT,BL}$ (fF)	420
$C_{IN,SH}$ (fF)	80	$C_{OUT,SH}$ (fF)	23
$C_{IN,BL}$ (fF)	420	$C_{OUT,BL}$ (fF)	420
$C_{FB,1}$, $C_{FB,2}$ (fF)	107	$R_{FB,1}$ (Ω)	1,028
$C_{INT,SH}$ (fF)	17	$R_{FB,2}$ (Ω)	771

[1)] total gate width

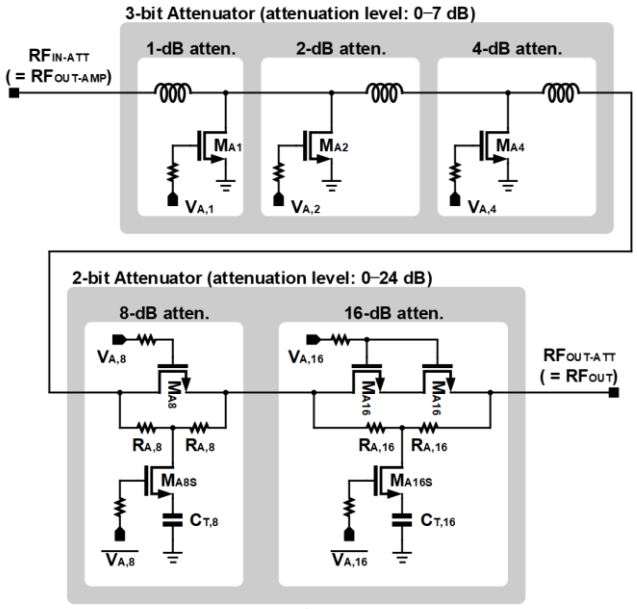

Fig. 3. Schematic of the attenuation stage.

described, and then the attenuator was described.

A. Two stage gain amplifier

As shown in Fig. 1, the proposed CMOS VGA consists of amplifiers and attenuators. Fig. 2 shows the schematic of the amplification stage constituting the designed VGA. The amplification stage is formed by connecting two common-source (CS) structures.

The gate bias voltages were applied through resistors, and the supply voltage, V_{DD} was 1.0 V. The stability of the entire amplification stage was secured through RC feedback technique. A capacitor was added between the drain and source of the transistor to reduce the size of the load inductor, thereby suppressing power loss caused by the inductor and reducing the overall chip size. Other capacitors were used as the role of the dc blocking and for matching. Additionally, an additional series inductor was also used for input matching. $RF_{OUT-AMP}$, which is an output signal of the amplification stage, becomes RF_{IN-ATT}, which is an input signal of the attenuator. Specific values of the devices used in the amplification stage are shown in Table I.

B. 5-bit Attenuator

The schematic of the 5-bit attenuator is shown in Fig. 3. In order to minimize insertion loss, the lower three bits were designed with a distributed structure. Thanks to the repeated structure of series inductance and shunt capacitance of the distributed structure, bandwidth degradation caused by the lower three bits was minimized [12–16]. In addition, compared to M_{A4} in Fig. 3 for 4 dB attenuation, M_{A1} for 1 dB attenuation and M_{A2} for 2 dB attenuation are designed to have relatively small gate width. This means that the parasitic capacitances of M_{A1} and M_{A2} are smaller than that of M_{A4}. Therefore, in order to reduce the chip area, the parasitic capacitances of M_{A1} and M_{A2} were regarded as an integrated capacitance from the perspective of the composition of the distributed structure. Through this, the inductor between M_{A1} and M_{A2} was removed for the configuration of the distributed structure.

On the other hand, attenuators for attenuation of 8 dB and 16 dB are designed in a π-structure to secure high attenuation levels [17–19]. In general, the size of the shunt transistor in the π-structure to secure a high attenuation level is designed relatively larger than that of the transistor in the distributed structure. Therefore, in the π-structure, a phase variation occurs according to the attenuation level by a relatively large parasitic capacitance of the shunt transistor. In this study, to mitigate this, tail capacitors $C_{T,8}$ and $C_{T,16}$ were added as shown in Fig. 3.

RF_{IN-ATT}, which is an input signal of the amplification stage, is the same as $RF_{OUT-AMP}$, which is an output signal of the amplifier. Specific values of the devices used in the attenuation stage are shown in Table II.

TABLE II. Specific Values of the Devices Used in the Attenuation Stage.

Device	Value	Device	Value
M_{A1} (μm)	1.7[1)]	M_{A8S} (μm)	7.2[1)]
M_{A2} (μm)	6.1[1)]	M_{A16S} (μm)	28.0[1)]
M_{A4} (μm)	9.0[1)]	$C_{T,8}$ (fF)	400
M_{A8} (μm)	40[1)]	$C_{T,16}$ (fF)	800
M_{A16} (μm)	40[1)]	-	-

[1)] total gate width

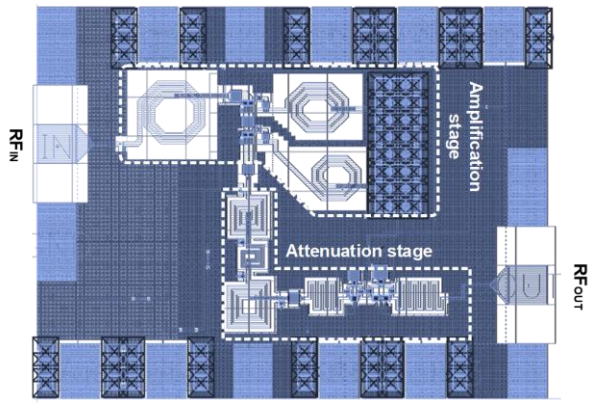

Fig. 4. Layout of the designed K-band CMOS VGA.

III. SIMULATION RESULTS OF THE K-BAND CMOS VGA

Fig. 4 shows the layout of the designed K-band CMOS VGA. The 65-nm RFCMOS process, which provides nine metal layers, was used. The areas of each of the amplification and attenuation stages are shown in Fig. 4. As shown in Fig. 4, in consideration of the connection with other circuits constituting each transceiver channel of the beamforming system, the attenuation stage was arranged in a bent form. Therefore, in the case of the test chip shown in Fig. 4, the

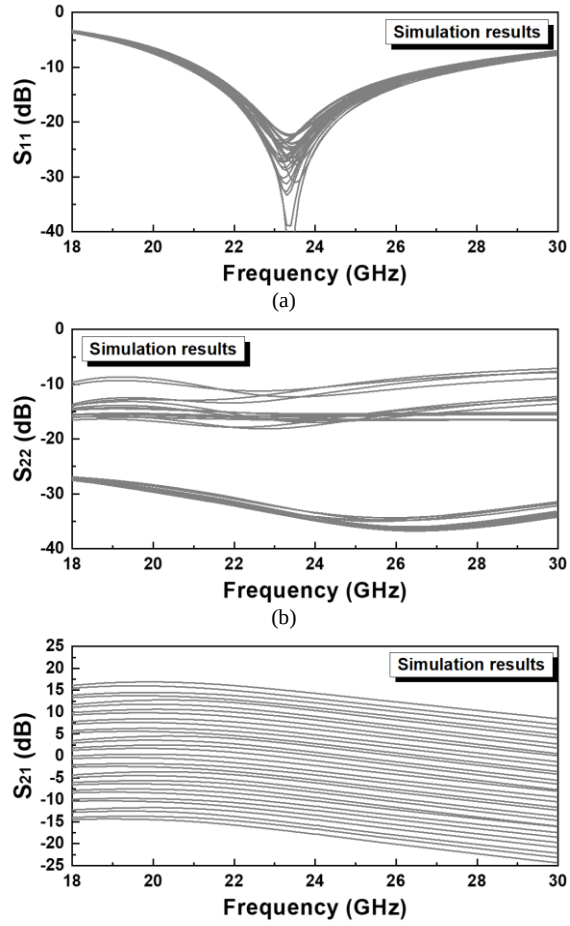

Fig. 5. Simulation results of S-parameters: (a) S_{11}, (b) S_{22}, and (c) S_{21}.

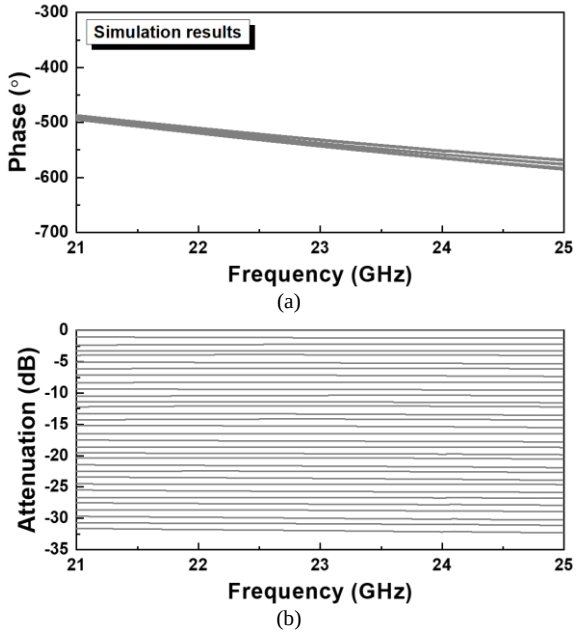

Fig. 6. Simulation results of phase and attenuation: (a) phase and (b) attenuation.

chip size increased due to the empty space where no devices and signal lines were placed. However, in the actual transceiver channel for beamforming system, other circuits were placed in the empty space of the designed test chip

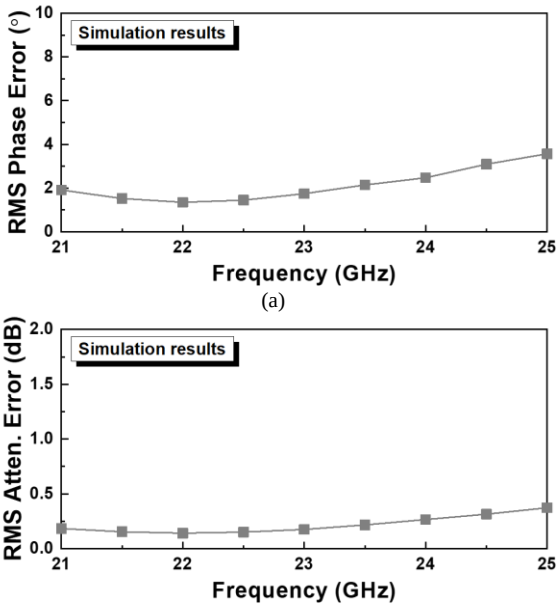

Fig. 7. Simulation results of RMS errors: (a) RMS phase and (b) RMS attenuation errors.

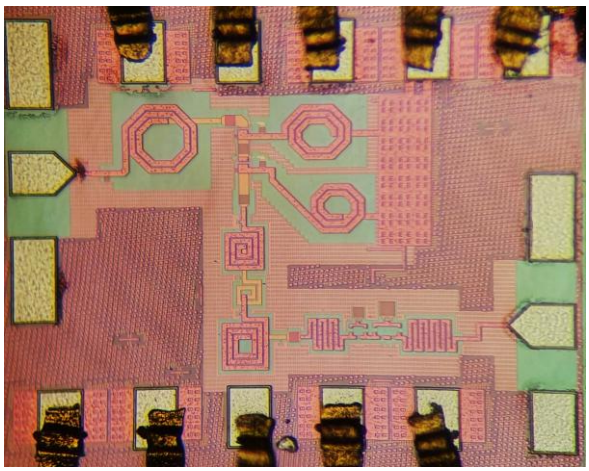

Fig. 8. Chip photograph of the designed K-band CMOS VGA.

shown in Fig. 4.

A supply voltage V_{DD} for the amplification stage is 1.0 V. In addition, the gate biases of the amplification stage, $V_{CS,1}$ and $V_{CS,2}$, are 0.55 V and 0.60 V, respectively. Control voltages V_{A1}, V_{A2}, V_{A4}, V_{A8}, and V_{A16} for adjusting the attenuation level are 0 V and 1 V. These supply voltage, gate biases, and control voltages were used equally not only in simulation but also in measurement.

To ensure the accuracy of the simulation, the effects of metal lines, inductors, and pads in the entire layout were considered through electromagnetic (EM) simulation. The target operating frequency range was 22.0 GHz to 23.6 GHz.

Fig. 5 shows the simulation results of the S-parameters. The target values of S_{11} and S_{22} were less than −10 dB. In the 21.0 GHz to 24.5 GHz range, which includes the target operating frequency range, both S_{11} and S_{22} were designed to be less than −10 dB. The degree of attenuation for each attenuation bit was confirmed from S_{21} of Fig. 5. The gain ranges at operating frequencies 22.0 GHz and 23.6 GHz were from 16.1 dB to −15.7 dB and 14.7 dB and −17.4 dB,

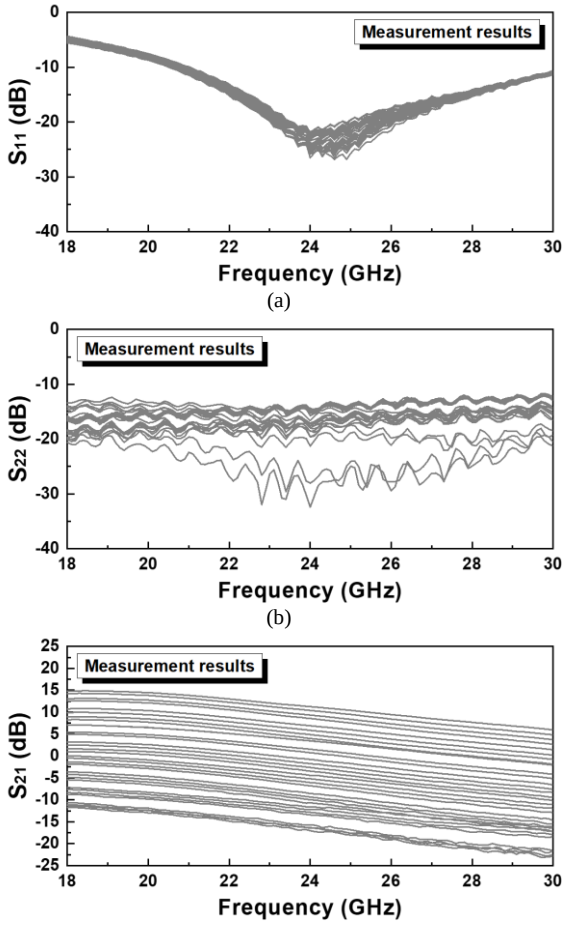

Fig. 9. Measurement results of S-parameters: (a) S_{11}, (b) S_{22}, and (c) S_{21}.

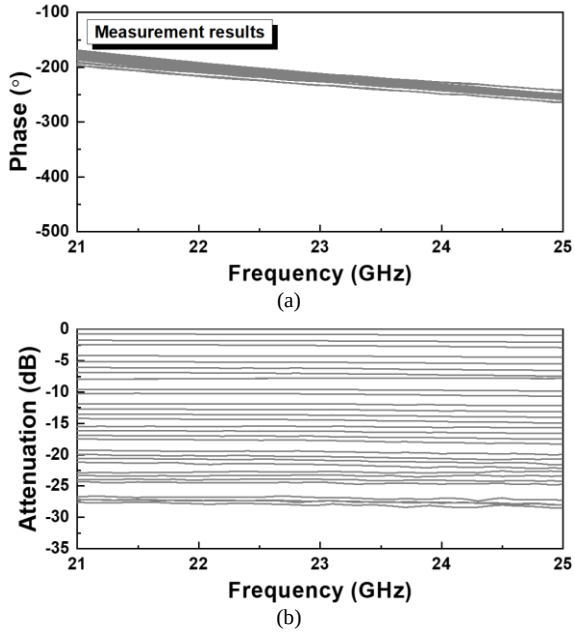

Fig. 10. Measurement results of phase and attenuation: (a) phase and (b) attenuation.

respectively. As a results, the variable gain ranges at operating frequencies 22.0 GHz and 23.6 GHz were 31.8 dB and 32.1 dB, respectively.

Fig. 6 shows the simulated phase and attenuation of each bit of the designed K-band CMOS VGA. At this time, Fig. 6(b) shows the simulated attenuation compared to the highest gain according to the frequency of the designed VGA. Fig. 7 shows the simulated RMS phase and attenuation errors derived based on the simulation results of the phase and attenuation shown in Fig. 6. From Fig. 7, in the operating frequency range of 22.0 GHz to 23.6 GHz, the RMS phase and attenuation errors were less than 2.25° and 0.22 dB, respectively.

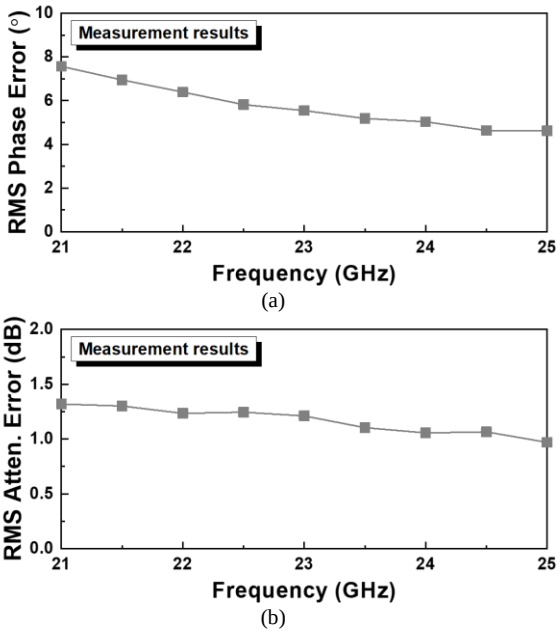

Fig. 11. Simulation results of RMS errors: (a) RMS phase and (b) RMS attenuation errors.

IV. MEASUREMENT RESULTS OF THE K-BAND CMOS VGA

Fig. 8 is a chip photograph of the designed K-band CMOS VGA. The total chip size, including the test pads, is 0.65 × 0.50 mm^2. RF input and output signals were measured using an RF probe on the wafer. Ground, supply voltage, gate biases, and control voltages were applied using bonding-wires.

Fig. 9 shows the measurement results of the S-parameters. The target values of S_{11} and S_{22} were less than −10 dB. In the 21.0 GHz to 30.0 GHz range, which includes the target operating frequency range, both S_{11} and S_{22} were designed to be less than −10 dB. The degree of attenuation for each attenuation bit was confirmed from S_{21} of Fig. 9. The gain ranges at operating frequencies 22.0 GHz and 23.6 GHz were from 13.0 dB to −14.9 dB and 11.6 dB and −16.6 dB, respectively. As a results, the variable gain ranges at operating frequencies 22.0 GHz and 23.6 GHz were 26.5 dB and 28.2 dB, respectively.

Fig. 10 shows the measured phase and attenuation of each bit of the designed K-band CMOS VGA. At this time, Fig. 10(b) shows the measured attenuation compared to the highest gain according to the frequency of the designed VGA. Fig. 11 shows the measured RMS phase and attenuation errors derived based on the measurement results of the phase and attenuation shown in Fig. 10. From Fig. 11, in the operating frequency range of 22.0 GHz to 23.6 GHz,

TABLE III. Performance Comparison with Various CMOS VGAs

Ref.	Tech. (nm)	Freq. (GHz)	Peak gain (dB)	Gain range (dB)	RMS phase error (°)
MWCL '19 [20]	65	30.0 – 34.5	20.8	10.6	< 3
MWCL '19 [21]	65	27.5	21.2	5	< 11 [1)]
MWCL '18 [22]	65	26 – 33	27.1	8.7	< 18 [1)]
APMC '20 [23]	65	24 – 28	29.4	6.2	< 3.3 [1)]
RFIC '18 [24]	65	27 – 42	9.6	7.8	< 3.5 [1)]
This work	65	22.0 – 23.6	13.0 – 11.6	26.5 – 28.2	< 6.40

[1)] maximum phase variation

the RMS phase and attenuation errors were less than 6.40° and 1.24 dB, respectively. The measured RMS errors were somewhat deteriorated compared to the simulation results. It is presumed that the main cause of deterioration is not only due to process variation, but also to the accuracy of electromagnetic simulation.

As shown in Table III, despite the wide range of gain variations, the measured RMS phase error characteristics are acceptable.

V. CONCLUSIONS

In this study, a K-band CMOS variable gain amplifier was designed. In order to secure power gain, two common-source gain stages were designed. In addition, in order to vary the gain, a variable attenuation stage that can be controlled with a total of 5-bits was designed. The distributed structure and π-structure were applied to the attenuation stage to suppress insertion loss and secure a wide variable attenuation range. The designed K-band VGA was fabricated using a 65-nm RFCMOS process. The chip size of the fabricated VGA was 0.65×0.50 mm^2. The variable gain range measured at operating frequencies 22.0 GHz to 23.6 GHz was from 26.5 dB to 28.2 dB. In the same frequency range, the measured RMS phase and attenuation errors were less than 6.40° and 1.24 dB, respectively.

ACKNOWLEDGMENT

The chip fabrication and EDA tool were supported by the IC Design Education Center(IDEC), Korea. This work was supported in part by the National Research Foundation of Korea (NRF) through the Korea government (MSIT) under Grant NRF-2021R1A2C1013666 and in part by the National Research Foundation of Korea (NRF) through the Korea Government (MSIT) under Grant NRF-2021R1A4A1032580.

REFERENCES

[1] B. S. Bae and J. H. Han, "A Wideband CMOS Down-conversion Mixer for 5G FR2 Applications," *Journal of Integrated Circuits and Systems*, vol. 8, no. 3, Jun. 2022.

[2] G. W. Park, S. J. Lee, J. M. Myung, H. Kim, and I. K. Nam, "A Millimeter-wave Up-converter for 28-GHz 5G Mobile Systems in 65-nm CMOS Technology," *Journal of Integrated Circuits and Systems*, vol. 9, no. 1, Jan. 2023.

[3] X. Hu, Y. Yi, K. Li, H. Zhang, and C. Kai, "Secure Transmission Design for Virtual Antenna Array-Aided Device-to-Device Multicast Communications," *IEEE Transactions on Wireless Communications*, vol. 22, no. 7, pp. 4814-4827, July 2023.

[4] L. Canese, *et al.*, "Efficient Digital Implementation of a Multirate-Based Variable Fractional Delay Filter for Wideband Beamforming," *IEEE Transactions on Circuits and Systems II: Express Briefs*, vol. 70, no. 6, pp. 2231-2235, June 2023.

[5] H. Jeong, H. D. Lee, B. Park, S. Jang, S. Kong, and C. Park, "Three-Stacked CMOS Power Amplifier to Increase Output Power with Stability Enhancement for mm-Wave Beamforming Systems," *IEEE Transactions on Microwave Theory and Techniques*, vol. 71, no. 6, pp. 2450-2464, June 2023.

[6] S. Jang, J. Lee, and C. Park, "K-band CMOS Low-noise Amplifier with 180° Phase Shift Function Using Cascode Structure," *Electronics Letters*, vol. 59, no. 15, e12908, Aug. 2023.

[7] S. Jang, C.-Y. Kim, and C. Park, "Design Technique of K-Band CMOS Phase Shifter with L-C-L T-Type Low Pass Structure," *Electronics*, vol. 12, no. 17, p. 3678, Aug. 2023.

[8] P. Guan et al., "A 33.5–37.5-GHz Four-Element Phased-Array Transceiver Front-End with Hybrid Architecture Phase Shifters and Gain Controllers," *IEEE Transactions on Microwave Theory and Techniques*, vol. 71, no. 9, pp. 4129-4143, Sept. 2023.

[9] O. Kazan, Z. Hu, L. Li, A. Alhamed, and G. M. Rebeiz, "An 8-Channel 5–33-GHz Transmit Phased Array Beamforming IC with 10.8–14.7-dBm Psat for C-, X-, Ku-, and Ka-Band SATCOM," *IEEE Transactions on Microwave Theory and Techniques*, vol. 71, no. 5, pp. 2029-2039, May 2023.

[10] J. G. Lee, T. H. Jang, G. H. Park, H. S. Lee, C. W. Byeon, and C. S. Park, "A 60-GHz Four-Element Beam-Tapering Phased-Array Transmitter with a Phase-Compensated VGA in 65-nm CMOS," *IEEE Transactions on Microwave Theory and Techniques*, vol. 67, no. 7, pp. 2998-3009, July 2019.

[11] B. Wang, H. Gao, A. R. van Dommele, M. K. Matters-Kammerer, and P. G. M. Baltus, "60-GHz Low-Noise VGA and Interpolation-Based Gain Cell in a 40-nm CMOS Technology," *IEEE Transactions on Microwave Theory and Techniques*, vol. 67, no. 2, pp. 518-532, Feb. 2019.

[12] D. P. Nguyen, B. L. Pham, and A. -V. Pham, "A 1.5–45-GHz High-Power 2-D Distributed Voltage-Controlled Attenuator," *IEEE Transactions on*

Microwave Theory and Techniques, vol. 65, no. 11, pp. 4208-4217, Nov. 2017.
[13] H. Kondoh, "DC-50 GHz MMIC Variable Attenuator with a 30 dB Dynamic Range", *in IEEE MTT-S International Microwave Symposium Digest*, New York, NY, USA, pp. 499-502, Jun. 1988.
[14] A. Sun, *et al.*, "A 26-32GHz Differential Attenuator with 0.23dB RMS Attenuation Error and 11.2dBm IP1dB in 40nm CMOS Process," in I*EEE/MTT-S International Microwave Symposium - IMS 2023*, San Diego, CA, USA, pp. 178-181, Jun. 2023.
[15] Z. Zhang, *et al.*, "A DC–Ka-Band 7-Bit Passive Attenuator with Capacitive-Compensation-Based Bandwidth Extension Technique in 55-nm CMOS," *IEEE Transactions on Microwave Theory and Techniques*, vol. 69, no. 8, pp. 3861-3874, Aug. 2021.
[16] B. Suh and B. -W. Min, "A 20–36-GHz Voltage-Controlled Analog Distributed Attenuator with a Wide Attenuation Range and Low Phase Imbalance," *IEEE Transactions on Microwave Theory and Techniques*, vol. 69, no. 5, pp. 2485-2493, May 2021.
[17] J. Bae, J. Lee, and C. Nguyen, "A 10–67-GHz CMOS Dual-Function Switching Attenuator with Improved Flatness and Large Attenuation Range," *IEEE Transactions on Microwave Theory and Techniques*, vol. 61, no. 12, pp. 4118-4129, Dec. 2013.
[18] B. -H. Ku and S. Hong, "6-bit CMOS Digital Attenuators with Low Phase Variations for X-Band Phased-Array Systems," *IEEE Transactions on Microwave Theory and Techniques*, vol. 58, no. 7, pp. 1651-1663, July 2010.
[19] M. Davulcu, C. Caliskan, I. Kalyoncu, M. Kaynak, and Y. Gurbuz, "7-Bit SiGe-BiCMOS Step Attenuator for X-Band Phased-Array RADAR Applications," *IEEE Microwave and Wireless Components Letters*, vol. 26, no. 8, pp. 598-600, Aug. 2016.
[20] S. Lee, J. Park, and S. Hong, "A Ka-Band Phase-Compensated Variable-Gain CMOS Low-Noise Amplifier," *IEEE Microwave and Wireless Components Letters*, vol. 29, no. 2, pp. 131-133, Feb. 2019.
[21] C. W. Byeon, S. H. Lee, J. H. Lee, and J. H. Son, "A Ka-Band Variable-Gain Amplifier with Low OP1dB Variation for 5G Applications," *IEEE Microwave and Wireless Components Letters*, vol. 29, no. 11, pp. 722-724, Nov. 2019.
[22] M. Elkholy, S. Shakib, J. Dunworth, V. Aparin, and K. Entesari, "A Wideband Variable Gain LNA with High OIP3 for 5G Using 40-nm Bulk CMOS," *IEEE Microwave and Wireless Components Letters*, vol. 28, no. 1, pp. 64-66, Jan. 2018.
[23] Q. Zhang, C. Zhao, Y. Yu, H. Liu, Y. Wu, and K. Kang, "A Ka-Band CMOS Variable Gain Amplifier with High Gain Resolution and Low Phase Variation," in *2020 IEEE Asia-Pacific Microwave Conference (APMC)*, Hong Kong, Hong Kong, 2020, pp. 275-277.
[24] Y. Yi, D. Zhao, and X. You, "A Ka-band CMOS Digital-Controlled Phase-Invariant Variable Gain Amplifier with 4-bit Tuning Range and 0.5-dB Resolution," 2018 IEEE Radio Frequency Integrated Circuits Symposium (RFIC), Philadelphia, PA, USA, 2018, pp. 152-155.

Junhyuk Yang received the B.S. and M.S. degrees in electronic engineering from Soongsil University, Seoul, South Korea, in 2019 and 2021, respectively.

His research interests include wireless power transfer and millimeter wave integrated circuits.

Seongjin Jang received the B.S. and Ph.D. degrees in electronic engineering from Soongsil University, Seoul, South Korea, in 2016 and 2023, respectively. He is currently a Post-Doctoral Researcher with the School of Electronic Engineering, Soongsil University, where he has been involved in designing RF and millimeter-wave integrated circuits (ICs) for wireless communication systems.

His current research interests include millimeter-wave integrated circuits and systems in CMOS and GaN HEMT technologies.

Changkun Park received the B.S., M.S., and Ph.D. degrees in electrical engineering from the Korea Advanced Institute of Science and Technology (KAIST), Daejeon, South Korea, in 2001, 2003, and 2007, respectively. From 2007 to 2009, he was with the Advanced Design Team of the DRAM Development Division, Hynix Semiconductor Inc., Icheon, South Korea, where he was involved in the development of high-speed I/O interfaces of DRAM. In September 2009, he joined the Faculty of the School of Electronic Engineering, Soongsil University, Seoul, South Korea.

His research interests include RF and millimeter-wave circuits, RF CMOS power amplifiers, and wireless chip-to-chip communication and power transfers.